# Advanced 3D Monte Carlo algorithms for bio-photonic and medical applications

Lewis McMillan

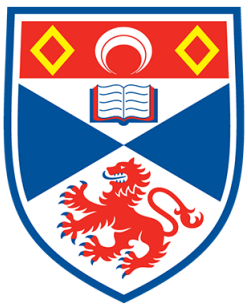

University of
St Andrews

This thesis is submitted in partial fulfilment for the degree of
PhD
at the
University of St Andrews

March 2019

# Contents

# List of Figures

# Chapter 1

# Monte Carlo radiation transport technique

## 1.1 Introduction and Background

This chapter will provide an overview of the Monte Carlo method and how it is used within the context of Monte Carlo radiation Transfer (MCRT). The chapter will then present the details of the MCRT code used as the basis of the subsequent chapters. Validation of this code and details of computational speed up are also presented. Subsequent chapters will expand upon the code for each individual projects needs.

### 1.1.1 Monte Carlo method

The Monte Carlo method is a numerical analysis technique based upon random numbers, which are used to calculate unknown variables in problems.

The earliest use of the method is in Buffon's needle experiment of the $18^{th}$ century [1–3]. Buffon asked the question;

"Suppose we have a floor made of parallel strips of wood, each the same width, and we drop a needle onto the floor. What is the probability that the needle will lie across a line between two strips?"

The solution to this question is as: for a needle length $l$, strip separation $s$, and where $x$ is the distance from the needle to the closest line. Then using a simple geometrical argument, a needle crosses a strip if $x \leq \frac{l}{2} sin\theta$.

$x$ is distributed uniformly in $[0, \frac{s}{2}]$, and $\theta$ in $[0, \frac{\pi}{2}]$. Therefore the probability density function for $x$ is $p(x) = \frac{2}{s}$, and $\theta$ is $p(\theta) = \frac{2}{\pi}$. The probability density function (PDF), is a function of a variable that gives probability for a variable to a take a given value. The PDF is normalised over the whole range of the variable, in this case $x$, and $\theta$. Thus, as $x$ and $\theta$ are independent variables, giving a joint probability of $p(x, \theta) = \frac{4}{s\pi}$. So the probability of a needle of length l ($l < s$) is:

$$P = \int_0^{\frac{\pi}{2}} \int_0^{\frac{l}{2} sin\theta} \frac{4}{s\pi} dx d\theta = \frac{2l}{s\pi} \tag{1.1}$$

Equation (1.1) can be used to carry out a Monte Carlo estimation of pi. A simple rearrangement yields: $\pi = \frac{2l}{sP}$ where P is the ratio of needles crossing the line over total number dropped.

Laplace was the first to suggest that Buffon's needle experiment could be used to estimate $\pi$ [2]. Figure 1.1 shows an example of simulation of Buffon's needle experiment.

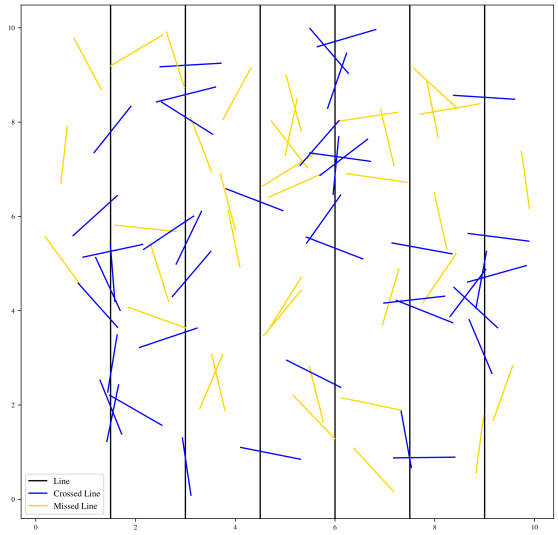


***Figure 1.1:*** *Sample buffon needle experiment. 100 needles are dropped on a 10 by 10 cm area with lines spaced 1.5cm apart. If a needle lands on a line it is recorded and coloured blue, else it is yellow. This simulation gave a value of pi as 3.17.*

The Monte Carlo method is used in various different disciplines. Ranging from use in the financial sector to analyse investments and stocks by simulating the sources of uncertainty which affect their values [4,5], use in statistical analysis [6], and in modern computer generated images (see Fig. 1.2) [7,8]. It is also widely used in astronomy and medicine, in order to simulate the propagation of particles through turbid media. This technique, Monte Carlo radiation transfer, is what makes up the bulk of this thesis and is described in depth in the following sections.

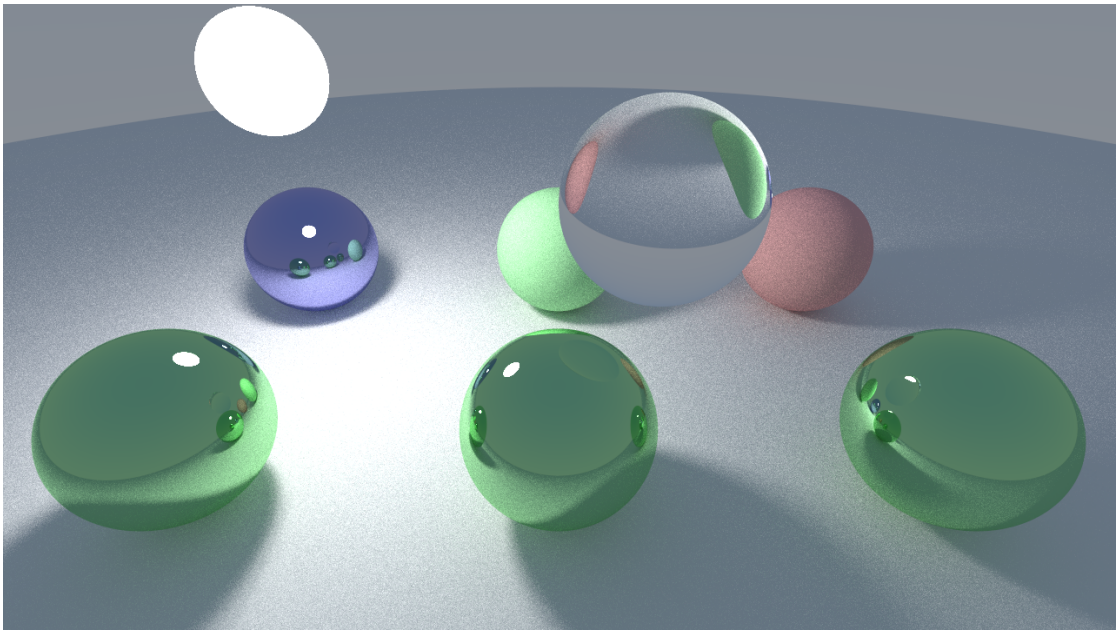

***Figure 1.2:*** *Computer generated imagery using ray-tracing. Code usd to create image available at:* https://github.com/lewisfish/RayTran

## 1.2 Monte Carlo radiation transport algorithm

### 1.2.1 Introduction & background

The technique that makes up the bulk of this thesis, is the MCRT technique. This method was developed at the tail end of the Second World War at the Los Alamos National Laboratory, for the purpose of calculating neutron diffusion though shielding material [9–12]. It has since found a myriad of applications from light transport through dusty clouds [13], calculating doses for radiotherapy [14] to light transport through tissue [15].***more here + link to next section***

#### 1.2.1.1 Radiative transfer

Transport of photons through turbid media, can be modelled analytically using the RTE. The RTE models the the radiative losses, and gains by a beam of radiation as it travels through a medium, including: loss of energy due to absorption, loss/gain of energy due to scattering, and energy gain due to emission. Before we derive the RTE, we first define some terms and physical quantities.

The first term is spectral irradiance, $L_\nu$. Spectral irradiance is defined as the energy flow in a direction $\mathbf{n}$, for a solid angle $d\Omega$, per unit time per unit temporal frequency bandwidth. Irradiance is defined as the spectral irradiance over a small frequency range $[\nu, \nu + \Delta\nu]$:

$$L(\vec{r}, \hat{s}, t) = L_\nu(\vec{r}, \hat{s}, t)\Delta\nu \tag{1.2}$$

Where:

$\vec{r}$ is the position;

$\hat{s}$ is the unit normal vector;

$t$ is the time;
and $L(\vec{r}, \hat{s}, t)$ is the irradiance $[W \cdot m^{-2} \cdot sr^{-1}]$.

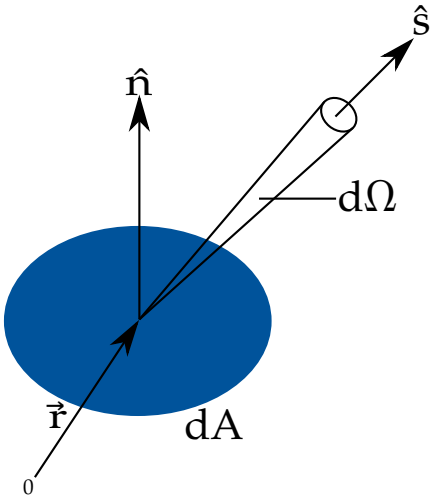


***Figure 1.3:*** *Energy flow through area $dA$ within solid angle $d\Omega$ in a direction $\hat{s}$. Adapted from [16, 17]*

The irradiance can be used to determine the energy, $dE$, transported across an area $dA$, in a solid angle $d\Omega$ in a time $dt$ (see Fig. 1.3) is:

$$dE = L(\vec{r}, \hat{s}, t) \cdot (\hat{s} \cdot \hat{n})\ dAd\Omega dt \tag{1.3}$$

Where:
$\hat{n}$ is the unit normal to $dA$;
and $\hat{s} \cdot \hat{n}$ is the angle of the solid angle.

Irradiance can also be used to determine the fluence rate, $\phi$, which is defined as the energy flow per unit time, independent of the flow direction.

$$\phi(\vec{r}, t) = \int_{4\pi} L(\vec{r}, \hat{s}, t)\ d\Omega \tag{1.4}$$

Where:
$\phi$ is the fluence rate $[W \cdot m^{-2}]$.

Irradiance is also the main variable in the RTE, as it describes the light distribution throughout the medium, and by solving the RTE yields the irradiance, which in turn gives information on the state of the system and all the physical properties of it.

With the irradiance defined, as well as the other quantities that follow, we can now derive the RTE [16, 17]. We first consider conservation of energy, as shown in Eq. (1.5).

$$dP = -dp_{div} - dp_{ext} + dP_{scatt} + dP_{src} \tag{1.5}$$

Where:
$dP$ is the total change in energy in the volume $dAds$ within the solid angle, $d\Omega$, per unit time (see Fig. 1.4);
$dP_{div}$ is the energy loss due to the divergence of the radiation beam per unit time;

$dP_{ext}$ is the energy loss due to absorption and scattering within $dAdsd\Omega$;
$dP_{scatt}$ is the energy gain due to scattering from $\hat{s}'$ into $d\Omega$ per unit time;
and $dP_{src}$ is the energy gain due to emission within the medium, per unit time.

The total change in energy in the volume element within the solid angle $d\Omega$, $dP$, is equal to:

$$dP = \frac{1}{c}\frac{\partial L(\vec{r},\hat{s},t)}{\partial t}\ dAdsd\Omega \tag{1.6}$$

Where c is the speed of light.

The first loss term, $dP_{div}$, is the energy loss due to divergence of the radiation beam. This is modelled as:

$$dP_{div} = \frac{\partial L}{\partial s}\ d\Omega dV \tag{1.7}$$
$$= \hat{s}\cdot\nabla L(\vec{r},\hat{s},t)\ d\Omega dV \tag{1.8}$$

$dP_{ext}$ is the second loss term, and accounts for energy loss due to scattering and absorption in the volume element within the solid angle $d\Omega$. This is modelled as:

$$dP_{ext} = \mu_t ds\ L(\vec{r},\hat{s},t)\ dAd\Omega \tag{1.9}$$

The first energy gain term, $dP_{src}$, is due to emission in the volume element within the solid angle $d\Omega$.

$$dP_{src} = S(\vec{r},\hat{s},t)\ dVd\Omega \tag{1.10}$$

The second energy gain term, and final term, is due to the incident energy on the volume element within the solid angle $d\Omega$ in direction $\hat{s}$ due to scattering from any direction $\hat{s}'$.

$$dP_{scatt} = N_s dV\left(\int_{4\pi} L(\vec{r},\hat{s}',t)P(\hat{s}',\hat{s})\sigma_s\ d\Omega'\right)\ d\Omega \tag{1.11}$$
$$= \mu_s dV\left(\int_{4\pi} L(\vec{r},\hat{s}',t)P(\hat{s}',\hat{s})\ d\Omega'\right)\ d\Omega \tag{1.12}$$

Where:
$N_s$ is the number density of scatters;
$P(\hat{s}',\hat{s})$ is the scattering phase function (see Section 1.4 for further discussion);
and $\sigma_s$ is the cross section of the scatters, thus $\mu_s = N_s\sigma_s$ (again see Section 1.4 for further discussion).

Finally substituting Eqs. (1.6), (1.8) to (1.10) and (1.12) into Eq. (1.5) yields the RTE:

$$\frac{1}{c}\frac{\partial L(\vec{r},\hat{s},t)}{\partial t} + s\cdot\nabla L(\vec{r},\hat{s},t) = -\mu_t L(\vec{r},\hat{s},t) + \mu_s\int_{4\pi} p(\hat{s},\hat{s}')L(\vec{r},\hat{s}',t)d\Omega' + S(\vec{r},\hat{s},t) \tag{1.13}$$

In general, the RTE is hard to solve in arbitrary 3D geometries, however there are a number of approximations, and numerical methods available. Diffusion approximation, Kubelka-Munk Theory (K-M theory), and MCRT are the common methods used to approximate the RTE.

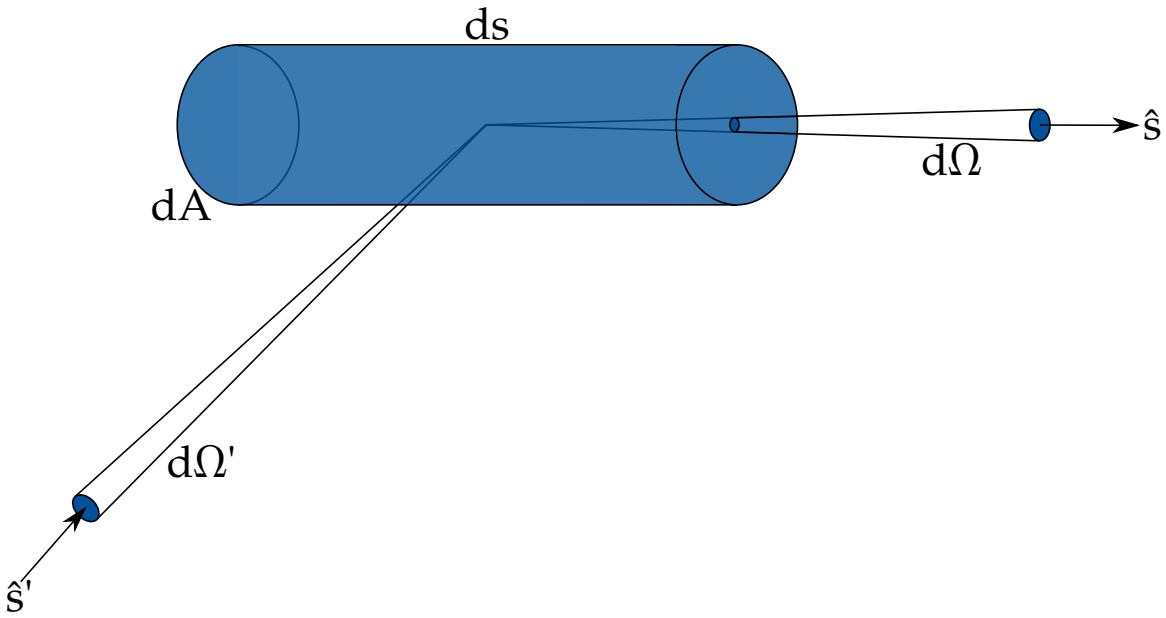


***Figure 1.4:*** *Cylindrical volume element, $ds \cdot dA$, with solid angle $d\Omega$ in direction $\hat{s}$ and solid angle $d\Omega'$ in direction $\hat{s}'$. Energy flowing through this element is used to derive the RTE. Adapted from [16, 17].*

**Kubelka-Munk theory** K-M theory was originally developed in order to calculate the light distribution in thin layered materials, such as paint or paper [18]. The theory is rather simple and makes many assumptions about the medium and the incident light. The main assumptions of K-M theory are: only scattering and absorption take pace in the medium, the incident light is already diffuse, the medium is uniform, only isotropic scattering, no external or internal reflections, and the medium is planar and infinitely wide [19–21].

These assumptions make K-M theory, very poor for modelling light-tissue interactions. This is as in tissue, scattering is not isotropic, but rather forward biased (see Section 1.4). Tissue is rarely, if ever, planar and infinitely wide. Tissue also has some reflections at its external and internal boundaries, due to change in refractive indices. Many medical and biophotonic treatments/methods use laser light which is not diffuse. Finally tissue can also exhibit fluorescence, which K-M theory is not able to model, along with polarization. K-M theory does have some positive aspects. It is good at calculating the diffuse reflectance of simple mediums, and can be used to roughly estimate calculations. Though it is not well suited for modelling light-tissue applications.***refs for these claims***

**Diffusion approximation** The diffusion approximation for the RTE, is where the irradiance is separated into two components:

$$L(\vec{r}, \hat{s}) = L_c(\vec{r}, \hat{s}) + l_d(\vec{r}, \hat{s}) \tag{1.14}$$

Where $L_c$ is the unscattered contribution, which satisfies Beer's law*, and $L_d$ is the diffuse contribution. The $L_d$ component is expanded using Legendre polynomials and truncated. The

*Beer's law (or Beer-Lambert law) states that the transmission, $T$, is equal to $e^{\mu L}$, where $L$ is the distance and $\mu$ is the attenuation coefficient.

diffusion approximation also has a number of assumptions and restrictions. The main assumption is that scattering dominates over absorption, and that the scattering is nearly isotropic. This restricts the types of scattering the Diffusion approximation can model, though using similarity relations can partially model scattering in tissue [22, 23].

Diffusion theory is computationally fast, and simple. However it is poor at modelling light-tissue interactions due to it's assumptions and restrictions, mainly the inaccurate modelling near the boundaries of the medium and its lack of modelling fluorescence and other microphysics. However it can be used to speed up MCRT in optically thick regions [24, 25].

The final method, MCRT, is a method that is numerically equivalent to the RTE [16]. MCRT is a very flexible method, it can model arbitrary 3D geometries, various microphysics: fluorescence, and polarisation. It can also model various different light sources, from collimated laser beams, to diffuse light sources. The only downside that is noted in the literature is that the MCRT can be very expensive computationally. However with computational power growing faster with each year, this is less and less of a problem going forward. The next several sections give an in depth description of the MCRT method and it's flexibility, along with a description of the code used in this thesis to solve various medical and biophotonic problems.

### 1.2.2 MCRT algorithm

The MCRT algorithm can be as simple as a $\sim$ 20 line program to as complex as needed for the problem at hand. This section will provide a detailed description a simple MCRT algorithm for a 3D voxel based grid.

#### 1.2.2.1 Grid set-up

The first step of the MCRT algorithm is to set-up the grid which acts as the simulated medium. This grid consists of $n \times n \times n$ voxels[†] of which each voxel has it's own optical properties (see Section 1.4 for discussion). This allows the medium of interest to be discretised onto a grid, which gives a good approximation of the real-life medium (see Section 1.5 for discussion on this). along with setting up the medium, arrays which store the locations of the voxel walls in each cardinal direction are created for reference in later parts of the code. Once the medium has been set-up photon packets are launched and propagated through the voxel structure.

#### 1.2.2.2 Photon launch

The initial step (besides medium set-up and other book keeping) of any MCRT algorithm is to launch a photon packet. Depending on the source of photon packets for a given simulation, this step varies from simulation to simulation. The general idea of launching a photon packet is that the packet is given an initial direction vector and position (which consists of a physical position and a voxel position)[‡]:

$$direction = \begin{bmatrix} n_{xp} \\ n_{yp} \\ n_{zp} \end{bmatrix} \tag{1.15}$$

$$position = \begin{bmatrix} x_p, y_p, z_p \end{bmatrix} \tag{1.16}$$

$$voxel = \begin{bmatrix} x_{cell}, y_{cell}, z_{cell} \end{bmatrix} \tag{1.17}$$

[†] A voxel is a 3D pixel

[‡] all variables given in this section are the same as they are in the code.

In order to set the direction vectors, the components of the direction vectors must be first set. The packets position is tracked using a Cartesian coordinate system, however for ease of computation for calculating scattering angles (see Section 1.2.2.4), the direction vectors are computed in a spherical system thus the direction vectors are:

$$n_{xp} = sin(\theta) \cdot cos(\phi) \tag{1.18}$$
$$n_{yp} = sin(\theta) \cdot sin(\phi) \tag{1.19}$$
$$n_{zp} = cos(\theta) \tag{1.20}$$

$\theta$ and $\phi$ are generated dependant on the photon source used. The individual sine and cosine terms are saved for use in the scattering routines, see Section 1.2.2.4.

#### 1.2.2.3 Photon move

The next step in the algorithm is moving a packet to the next interaction point. The probability a packet will interact over a distance $dL$ is $\mu_t dL$, where $\mu_t$ is the interaction probability (see Section 1.4). Thus the probability of travelling $dL$ without any interaction is $1 - \mu_t dL$. Therefore over a distance $L$, with N segments of length $L/N$ the probability of travelling $L$ before any interaction:

$$P(L) = (1 - \mu_t \frac{L}{N}) \cdot (1 - \mu_t \frac{L}{N}) \ldots (1 - \mu_t \frac{L}{N}) = (1 - \mu_t \frac{L}{N})^N \tag{1.21}$$
$$P(L) = \lim_{N \to \infty} (1 - \mu_t \frac{L}{N})^N = e^{-\mu_t L} = e^{-\tau} \tag{1.22}$$

Where $\tau$ is the number of mean free paths over a distance L. We now have a PDF, Eq. (1.22), for the distance a packet will travel before an interaction occurs. For this to be of use we need to be able to sample from this PDF in order to get a random optical depth. Using the Monte Carlo method described in Section 1.1.1, with $\xi$ as our random variable, we get:

$$\xi = \int_0^\tau e^{-\tau'} = 1 - e^{-\tau} \rightarrow \tau = -log(1 - \xi) \tag{1.23}$$

As $\xi$ is symmetric about 0.5 we can substitute $1 - \xi$ for $\xi$ yielding:

$$\tau = -log(\xi) \tag{1.24}$$

We now have an optical distance, however we need to convert this into a physical distance so that we can move our photon packet. From our definition of $\tau$ we know that $\tau = \int_0^L \mu_t dS$, and if we have a smooth, homogeneous medium (i.e not a gridded medium) thus

$$L = \frac{\tau}{\mu_t} \tag{1.25}$$

Therefore in order to update the packets position is simply:

$$x_p = x_p + L \cdot n_{xp} \tag{1.26}$$
$$y_p = y_p + L \cdot n_{yp} \tag{1.27}$$
$$z_p = z_p + L \cdot n_{zp} \tag{1.28}$$

However as the code in this thesis is a 3D gridded Cartesian code, we have to slightly adjust how we move and update the packets position. As stated in Section 1.2.2.1, the medium has been discretised onto a grid, so that each voxel can have a different $\mu_t$, thus Eq. (1.25) becomes:

$$L = \frac{\tau}{\mu_{t,\zeta}} \qquad \zeta = (x, y, z) \tag{1.29}$$

with $\mu_{t,\zeta}$ the $\mu_t$ for the $\zeta^{th}$ voxel. The position is then updated as before using Eqs. (1.26) to (1.28). The next step in the algorithm is the interaction event, which can consist of either: scattering, absorbing or fluorescing.

#### 1.2.2.4 Photon scatter and absorbing

The first part of this section of the algorithm is to decide what kind of interaction the packet has with the medium. This section will focus on scattering and absorbing with other interaction events left for the chapters that detail these behaviours.

To decide whether a packet scatters or absorbs involves 'throwing' a random number and comparing it against the albedo. As detailed in Section 1.4 the albedo is the scattering probability $a = \frac{\mu_a}{\mu_a + \mu_s}$. The random number is compared to the albedo, and if the random number is less than the albedo then the packet scatters, otherwise the packet is absorbed.

**Packet absorption**

If the interaction event is a photon packet absorption, then the algorithm terminates the photon packets and starts the next photon packet, Section 1.2.2.5.

**Packet scattering**

If the interaction event is a packet scattering, then the packet is scattered into a new direction and the above process are carried out until a termination clause is met, see Section 1.2.2.5.

Depending of the medium being simulated, it can either be isotropically scattering or preferentially scattering in a direction. In the case of simulating photon propagation in tissue, tissue is highly forward scattering.

Anisotropy is the degree of deviation in the photon packets path at each interaction event. The measure of anisotropy is the g value, $g$. With $g$ taking any value from $-1$ to 1, $-1$ is highly backward scattering, 0 is isotropic scattering and 1 is highly forward scattering.

#### 1.2.2.5 Termination

### 1.2.3 Code details

This section details the the actual implementation of the MCRT algorithm detailed in the previous section, along with any computational necessities and speed ups on the original algorithm.

## 1.3 Validation of MCRT code

## 1.4 Optical properties

Optical properties of a medium are the properties that determine how light is transported though that medium. Usually the optical properties of a medium are defined by four main parameters:

the scattering and absorption coefficients ($\mu_s$ and $\mu_a$), the anisotropy coefficient ($g$), and the refractive index ($n$). There are several other optical properties the medium can be defined with, however these in general are only used for specific applications, such as Raman cross-sections.

### 1.4.1 Scattering

The scattering coefficient, along with the anisotropy value (see Section 1.4.2), define how light is transported though a medium. Scattering in skin is due to a number of different scatterers, and inhomogeneities within the skin. The main scatterers are filamentous proteins such as collagen, and elastin which are generally found within the dermis, and epidermis and both are composed of long filament like bundles ***ref 7***. In the upper layers of the skin the main scatterers are keratins and various chromophores such as melanin. These scatterers and their size determine how light is scattered, and in which direction into.

The scattering of light within tissue is usually defined as $\mu_s$ or $\mu_s'$: the scattering coefficient and the reduced scattering coefficient, where $\mu_s' = \mu_s(1-g)$. The scattering coefficient is defined such that the probability of transmission without scattering in a path length L is:

$$T = e^{-\mu_s L} \tag{1.30}$$

This gives units of inverse length for the scattering coefficient (usually measured in $cm^{-1}$). The reduced scattering coefficient is quite often given in place of the scattering coefficient, as the reduced coefficient is more easily measured then the 'normal' coefficient [26].

### 1.4.2 Anisotropy

Anisotropy describes the degree of deviation in the photon path at each scattering event. The anisotropy value is taken from the phase function for the medium. The phase function, $\Phi(\theta, \phi)$, is usually normalised over all angles:

$$\int_\Omega \Phi(\theta, \phi)\ d\Omega = 1 \tag{1.31}$$

Where $\theta$, and $\phi$ are the usual spherical angles. Thus Rayleigh and isotropic scattering's phase functions are:

$$\Phi_{isotropic}(\theta, \phi) = \frac{1}{4\pi} \tag{1.32}$$

$$\Phi_{Rayleigh}(\theta, \phi) = \frac{3}{8\pi}(1 + cos^2(\theta)) \tag{1.33}$$

Phase functions are hard to experimentally determine for biological tissues ***ref***, therefore the phase function is usually cast as the anisotropy value g, which is defined as the average angle of deflection:

$$g = \langle cos(\theta) \rangle = \int_\Omega cos(\theta)\Phi(\theta, \phi)\ d\Omega \tag{1.34}$$

The anisotropy factor, g, can take on any value from $-1$ to 1. Where a value of $-1$ is highly backward scattering, 0 is isotopic scattering and 1 is highly forward scattering.

There are various phase functions that can be used to model the anisotropy factor in medium, but the standard phase function for scattering in a biological tissue is the Henyey-Greenstein phase function. The Henyey-Greenstein phase function is shown in Eq. (1.35):

$$\Phi_{H.G}(\theta, \phi) = \frac{1}{4\pi} \frac{1 - g^2}{(1 + g^2 - 2g\ cos(\theta))^{\frac{3}{2}}} \tag{1.35}$$

The Henyey-Greenstein phase function is regarded as a 'good' phase function for biological tissues as it can model forward scattering, which tissue exhibits, and it is relatively simple.

### 1.4.3 Absorption

The absorption within biological tissues is defined by the absorption coefficient $\mu_a$. The absorption coefficient is defined, like the scattering coefficient, by considering the probability of transmission without absorbing in a path length L:

$$T = e^{-\mu_a L} \tag{1.36}$$

This, again like the scattering coefficient, gives inverse distance for the unit of the absorption coefficient (and its is also usually measured in units of $cm^{-1}$).

### 1.4.4 Refractive index

### 1.4.5 Other parameters

## 1.5 Further extensions to the code

# Appendices

# Appendix A

# Heat equation derivation

To derive the heat equation we consider the conversation of energy in a volume R, with a flux out, $\phi(x, y, z, t)$, and unit outer normal $\hat{\mathbf{n}}$. We need just the normal component of $\phi$ : $\phi \cdot \hat{\mathbf{n}}$.

The rate of change of heat inside the volume R is equal to the heat generated inside the volume R plus the heat flowing in/out of the boundary surface:

$$\begin{array}{l}\text{Rate of change} \\ \text{of heat energy}\end{array} = \begin{array}{l}\text{Rate of heat} \\ \text{generation in} \\ \text{R}\end{array} + \begin{array}{l}\text{Rate of heat energy} \\ \text{flowing through bound-} \\ \text{ary surface}\end{array} \tag{A.1}$$

The total heat energy is:

$$e(x, y, z, t) = c(x, y, z) \cdot \rho(x, y, z) \cdot T(x, y, z, t) \tag{A.2}$$

and therefore the rate of change of heat energy is

$$\frac{d}{dt} \iiint_R e \; dV = \frac{d}{dt} \iiint_R c\rho T \; dV \tag{A.3}$$

We denote the heat generated inside the volume R as $Q(x, y, z, t)$:

$$\iiint_R Q \; dV \tag{A.4}$$

and the rate of heat energy flowing through the boundary surface is:

$$- \iint_{\partial R} \phi \cdot \hat{\mathbf{n}} \; dS^{\ddagger} \tag{A.5}$$

Substituting Eqs. (A.3) to (A.5) into Eq. (A.1), yields:

$$\frac{\partial}{\partial t} \iiint_R c\rho T \; dV = - \iiint_R \phi \cdot \hat{\mathbf{n}} \; dV + \iiint_R Q \; dV \tag{A.6}$$

Using the divergence theorem, and simplifying gives:

[‡]This is negative as outward flow $\phi$ is positive, but the flow would result in a reduction of energy.

$$\frac{\partial}{\partial t}\iiint_R c\rho T \; dV = -\iiint_R \nabla \cdot \phi \; dV + \iiint_R Q \; dV \tag{A.7}$$

$$\iiint_R \left[ c\rho \frac{\partial}{\partial t} T + \nabla \cdot \phi - Q \right] dV = 0 \tag{A.8}$$

Which holds for an arbitrary R, thus:

$$c\rho \frac{\partial}{\partial t} T = -\nabla \cdot \phi + Q \tag{A.9}$$

Using Fourier's law of heat conduction, which states that the local heat flux density, $\phi$, is proportional to the negative local temperature gradient. The proportionality constant being equal to the thermal conductivity, $\kappa$:

$$\phi(x, y, z, t) = \kappa(x, y, z) \nabla T(x, y, z, t) \tag{A.10}$$

Substituting Eq. (A.10) into Eq. (A.9) yields the heat equation:

$$c\rho \frac{\partial}{\partial t} T = \nabla \cdot (\kappa \nabla T) + Q \tag{A.11}$$

Which can be simplified into the homogeneous medium heat equation with the following assumptions: Q=0 and $\kappa$, $\rho$, *and* $c$ are constant, and $\alpha = \frac{\kappa}{c\rho}$

$$\frac{\partial T}{\partial t} = \alpha \nabla^2 T \tag{A.12}$$

# Bibliography


[1] Lee Badger. Lazzarini's lucky approximation of $\pi$. *Mathematics Magazine*, 67(2):83–91, 1994.

[2] Petr Beckmann. *A history of Pi*. St. Martin's Griffin, 2015.

[3] Georges-Louis Leclerc Buffon. *Histoire naturelle générale et particulière*, volume 18. de l'Imprimerie de F. Dufart, 1785.

[4] Peter Jäckel. *Monte Carlo methods in finance*. J. Wiley, 2002.

[5] David B Hertz. Risk analysis in capital investment. *Harvard Business Review*, 42(1):95–106, 1964.

[6] Jasper Vivian Wall and Charles R Jenkins. *Practical statistics for astronomers*. Cambridge University Press, 2012.

[7] James T. Kajiya. The rendering equation. *SIGGRAPH Comput. Graph.*, 20(4):143–150, August 1986.

[8] Robert L. Cook, Thomas Porter, and Loren Carpenter. Distributed ray tracing. *SIGGRAPH Comput. Graph.*, 18(3):137–145, January 1984.

[9] Nicholas Metropolis. The beginning of the Monte Carlo method. *Los Alamos Science*, 15:125–130, 1987.

[10] Roger Eckhardt. Stan Ulam, John von Neumann, and the Monte Carlo method. *Los Alamos Science*, 15:131–136, 1987.

[11] HL Anderson. Metropolis, Monte Carlo, and the MANIAC. *Los Alamos Science*, 14:96–108, 1986.

[12] Stanislaw Ulam, RD Richtmyer, and J Von Neumann. Statistical methods in neutron diffusion. *LAMS-551, Los Alamos National Laboratory*, pages 1–22, 1947.

[13] Kenneth Wood and RJ Reynolds. A model for the scattered light contribution and polarization of the diffuse h$\alpha$ galactic background. *The Astrophysical Journal*, 525(2):799, 1999.

[14] DWO Rogers, BA Faddegon, GX Ding, C-M Ma, J We, and TR Mackie. Beam: a monte carlo code to simulate radiotherapy treatment units. *Medical physics*, 22(5):503–524, 1995.

[15] BC Wilson and G Adam. A monte carlo model for the absorption and flux distributions of light in tissue. *Medical Physics*, 10(6):824–830, 1983.

[16] Lihong V Wang and Hsin-i Wu. *Biomedical optics: principles and imaging*. John Wiley & Sons, 2012.

[17] Subrahmanyan Chandrasekhar. *Radiative transfer*. Courier Corporation, 2013.

[18] Vesna Džimbeg-Malčić Željka Barbarić-Mikočević and Katarina Itrić. Kubelka-munk theory in describing optical properties of paper (i). *Technical Gazette*, 18(1):117–124, 2011.

[19] Marek Jasiński. Modelling of light and human skin interaction using kubelka-munk theory. *Scientific Research of the Institute of Mathematics and Computer Science*, 10(1):71–81, 2011.

[20] Wai-Fung Cheong, Scott A Prahl, and Ashley J Welch. A review of the optical properties of biological tissues. *IEEE journal of quantum electronics*, 26(12):2166–2185, 1990.

[21] Macaveiu Gabriela. Mathematical methods in biomedical optics. *ISRN Biomedical Engineering*, 2013, 2013.

[22] Reindert Graaff, Jan G Aarnoudse, Frits FM de Mul, and Henk W Jentink. Similarity relations for anisotropic scattering in absorbing media. *Optical engineering*, 32(2):244–253, 1993.

[23] Gilwon Yoon, Scott A Prahl, and Ashley J Welch. Accuracies of the diffusion approximation and its similarity relations for laser irradiated biological media. *Applied Optics*, 28(12):2250–2255, 1989.

[24] Thomas P Robitaille. On the modified random walk algorithm for monte-carlo radiation transfer. *Astronomy & Astrophysics*, 520:A70, 2010.

[25] M Min, CP Dullemond, C Dominik, Alex de Koter, and JW Hovenier. Radiative transfer in very optically thick circumstellar disks. *Astronomy & Astrophysics*, 497(1):155–166, 2009.

[26] Steven L Jacques. Optical properties of biological tissues: a review. *Physics in Medicine & Biology*, 58(11):R37, 2013.